Fiber loop resonator sensor achieved by high-scattering MgO nanoparticle-doped fibers

Carlo Molardi, Wilfried Blanc, Daniele Tosi

Fiber loop resonator sensor achieved by high-scattering MgO nanoparticle-doped fibers

Carlo Molardi [a,*], Wilfried Blanc [b], Daniele Tosi [a,c]

[a] Nazarbayev University, School of Engineering and Digital Sciences, 53 Kabanbay Batyr, 010000, Nur-Sultan, Kazakhstan
[b] Université Côte D'Azur, Institut de Physique de Nice, CNRS UMR 7010, Parc Valrose, 06108, Nice, France
[c] National Laboratory Astana, Laboratory of Biosensors and Bioinstruments, 53 Kabanbay Batyr, 010000, Nur-Sultan, Kazakhstan

ARTICLE INFO

Keywords:
Fiber optic sensors (FOS)
Distributed sensors
Optical frequency-domain reflectometry (OFDR)
High scattering fibers
Nanoparticle doped fibers
Biomedical sensors

ABSTRACT

A Sagnac loop-based fiber sensor has been built using a special MgO-based nanoparticle doped fiber. The fiber presents a backscattering of 39.5 dB higher with respect to a standard SMF-28 telecom fiber. The backscattering properties of the fiber, combined with a locally stable polarization pattern, have fostered a clear interferometer pattern in middle point of the loop, presenting a backscattering peak roughly 78 dB higher with respect to a standard SMF-28 telecom fiber. The interferometer spectrum, showing a noisy nature given by the presence of the NP-doped fiber element, is clearly detectable. The loop-based sensor has been investigated by changing temperature and strain. The interferometer spectrum shows a shift, detectable with peak tracking and/or correlation method, toward the longer wavelength when temperature and applied strain increase. The measured coefficient of temperature and strain are respectively 1.75 p.m./°C and 1.93 p.m./με. This system shows interesting perspective for combining different optical fiber devices, in order to achieve simultaneous detection and discrimination of temperature and strain.

1. Introduction

In the scientific community, the use of Optical fiber sensors (OFS) is highly regarded as a versatile technology, combining a large applications pool and high-performing sensing [1,2]. The reason of the success of OFS can be identified in several factor including: the compact form factor and size, the capability of long-range sensing, the immunity to the external electromagnetic interference, and the intrinsic robustness, which permits the use of OFS in harsh environment [3]. However, the capability of OFS is not limited to the environmental sensing, OFS technology finds an interesting and growing position in the bio-medical sector. This is mainly because OFS, usually built of silica glasses, are biocompatible (according ISO 10993 standard [4]), permitting safe and minimally invasive treatments [5].

The main target of OFS, in terms of measurable physical properties, is the measurement of temperature and strain [6]. Nevertheless, adding microfabrication to the sensors, using optical transducers, or exploiting the properties of specialty fibers like Photonics Crystal Fibers (PCF), other measurables can be detected, such as pressure, force, refractive index, and chemicals [7–10].

Modern OFS based systems come in a variety of possible configurations, ranging from a more classical single point sensing, based on Fiber Bragg Grating (FBG) technology, to more complex sensing systems exploiting the techniques of multipoint, semi-distributed and distributed sensing [11,12]. With techniques of multiplexing and distributed sensing, a large number of sensing points can be located in small areas, thus increasing the sensing density. Distributed sensing is obtained by implementing the principles of Optical Frequency-Domain Reflectometry (OFDR). Exploiting the natural occurring Rayleigh scattering presents in the fiber, it is possible to sense changes of temperature and strain as a shift of the deterministic backscattering spectra that characterize each fiber, point by point [13]. The technological implementation of this method is the optical backscatter reflectometer (OBR), conceptualized and industrialized by Luna [14]. Recently, an improvement in this field has been demonstrated by extending the distributed sensing to a network of parallel fiber sensors, exploiting the concept of Scattering Level Multiplexing (SLMux) [15,16]. Here, special nanoparticles (NP) doped fibers, presenting a larger backscattering [17], are used to create diversity in the backscattering intensity to select and discriminate the correct sensing point in the parallel setup. The use of high scattering NP-doped fiber is not limited to multiplexing but can be extended to the concept of reflector-less sensing for refractive index and

* Corresponding author.
E-mail address: carlo.molardi@nu.edu.kz (C. Molardi).

bio sensors [18].

While FBGs based sensors represent a compact and cost-effective solution in terms of single and multi-point sensing, and the OBR based sensing systems represent a revolution in terms of sensing density, a third family of fiber sensors shows higher performance in terms of sensitivity. This family is based on fiber interferometers [2,19], where the measurable physical parameters influence the spectral response of the sensors. Many possible interferometer configurations have been proposed to achieve sensing in intrinsic and extrinsic structures, in between them, the Sagnac interferometers and loop-based resonator represent a particularly interesting solution. Fiber loop resonator presents the advantage to be a simple structure, with an intrinsic environmental robustness. It is also easy to fabricate since the loop is obtained by closing the sensing element in a loop between the ends of a 50:50 fiber coupler [20]. Even if fiber loop resonators find their main application in optical fiber-based gyroscope system, permitting a level of precision unreachable with inertial gyroscopes [21], other sensing applications are possible. These applications include temperature, strain, acoustic and chemical sensing [22–25].

In this work a fiber loop resonator system has been combined with the OBR technology. Moreover, for the sensing element in the fiber loop, the NP-doped fiber has been chosen. The high-backscattering properties of the NP-doped fiber permits the formation of an interference pattern detectable by the OBR system. The interference spectrum presents the noise typical of the high scattering, induced by the random pattern of nanoparticles included in the fiber core. The detection is fostered by the high backscattering peak formed in the loop location where the clockwise and the counterclockwise signals encounter each other. The spectrum of the backscattering peak has been investigated in presence of temperature and strain variations. The results, in terms of spectral shift, have been discussed.

2. Nanoparticles doped fibers

2.1. Fabrication and properties

The special fiber used for this work is characterized by a core with MgO-based nanoparticles. The fiber is fabricated with the drawing process described in Refs. [17,26,27]. The preform is obtained by a conventional MCVD (Modified Chemical Vapor Deposition) process, a simple and reliable technique suitable for the production of silica-based specialty fibers. The chemical principle, which permits the formation of nanoparticles is based on spontaneous phase separation process. In fact, a system composed by silicate shows immiscibility when it contains alkaline earths in form of oxide. No additional heat treatment is required to the achieve the growth of nanoparticles rich of MgO. Since the process is based on chemical separation, final size and distribution of nanoparticles are quite random and dependent on the Mg concentration in the preform [28].

Regarding the preform recipe, a germanium doped silica porous layer has been deposited inside a silica tube at a temperature of 1600 °C. The layer has been soaked three times in a 5 ml doping solution injected in the tube. The solution is ethanol-based and contains 0.1 mol/l of $MgCl_2$ for R04 and 10^{-4} mol/l of $ErCl_3$ and 0.1 mol/l of $MgCl_2$ for M01. The porous layer has been dried and sintered at a temperature of 1860 °C. Finally, the tube has been collapsed into the preform. Using this preform, a fiber, presenting the typical telecom fiber size (cladding diameter of 125 μm and a core diameter of roughly 10 μm), has been drawn using a drawing tower. The standard size and the fact that the presence of nanoparticles in the core does not drastically change the mechanical properties of the silica substrate, permits an easy splicing with standard SMF-28 fibers.

The presence of nanoparticles, their distribution and their size, significantly increase the scattering in the fiber. Just to have an idea, Fig. 1(a) and (b) shows the backscattering traces measured by the Luna OBR, of some samples of NP-doped fiber. Both traces depict a sawtooth shape, with an increasing of backscattering after the splice with the SMF-28 pigtail and an attenuation slope after the backscattering gain. The parameters of scattering gain and attenuation are dependent on the nanoparticle statistics (size and distribution). In Fig. 1(a) is shown the fiber tagged as M01, presenting a scattering gain of 44.5 dB and a two-way losses of 35.4 dB/m, while in Fig. 1(b) is shown the fiber tagged as R04, presenting a gain of 39.3 dB and a two-way losses of 134 dB/m. The gain and the losses are different since their content of nanoparticles is different. The term “two-way losses” is used to indicate that the losses are measured on a path that is double with respect to the output length, shown by Luna OBR. This is because the Luna input laser signal goes forth and returns to the instrument, so that the attention is accumulated on a double length. The loss values shown in Fig. 1, and measured in dB/m, represent 2α, where α is the one-way loss coefficient of the fiber.

Both the M01 and R04 present a core uniformly doped with Mg based nanoparticles. The preform recipe for M01 and R04 are the same, the main difference is that M01 presents Erbium in the core while R04 does not. Fiber draw is uniform, except for the fact that it induces elongation and break-up of particles. The different scattering properties of the fibers are due to the preforms, which are not longitudinally homogeneous. The preform can be homogeneous on 1 cm, but variations can occur for longer length due to the specific doping process.

2.2. Modal properties of NP-doped fiber

In the germanium-doped silica based preform fabrication, the formation of oxide nanoparticles is fostered by the high temperature of the process. The chemical principle of phase separation creates two phases in the core of the fiber: one rich of silica and one rich of MgO, condensed to form spherical nanoparticles. Unfortunately, the final composition of the preform is difficult to estimate, as well as the exact composition of the particles [17]. The strong scattering, induced by the nanoparticles, makes difficult the experimental characterization of the core refractive index by using a preform analyzer. However, some estimations can be done. The refractive index contrast of the core substrate is roughly estimated to a value of 1.7×10^{-3}, based on the averaged concentration of germanium used in the preform fabrication. According to the concentration of magnesium, the refractive index of the nanoparticles can vary from 1.53 to 1.65. The size and the concentration of the particles can be estimated by analyzing the cross-section of the fiber. The nanoparticles size varies from 20 to 100 nm, while the concentration varies form 1.2×10^{19} to 6.8×10^{19} particles/m^3.

Because the presence of the nanoparticles, that can induce phenomenon of localization in the core, the fiber modal properties are difficult to predict. A numerical analysis has been performed by the help of COMSOL Multiphysics, a commercial Finite Element Method (FEM) based simulation software. Several structures with random nanoparticles distribution have been taken in consideration. On each of them a modal analysis has been performed at a wavelength of 1550 nm. Some of the results are shown in Fig. 2(a)-(f). The fiber appears to sustain few modes, in particular a Fundamental Mode (FM) which assumes the shape of the LP_{01}, and a Higher Order Mode (HOM) which resembles the LP_{11}. The modes are clearly distorted by the presence of the nanoparticles, moreover, the nanoparticles induce a good confinement of the FM, while they reject the first HOM in peripheral area of core toward the cladding. To quantify the confinement the core overlap parameter Γ has been used. The overlap parameter represents the modal intensity integrated over the core area normalized to the total power of the mode.

From the analysis of the overlap parameter it is possible to see that the FM presents, also in the worst cases, an overlap higher than 0.82, while the most confined HOM found presents an overlap lower than 0.34. A low overlap is usually associated to poor guidance properties, so that the propagation of the HOM, which technically exists in the structure, is practically impeded. The structure, *de facto*, behaves like a single mode fiber. An experimental evidence of this behavior can be retrieved in Ref. [29], where the NP-doped fiber has been used as a support to

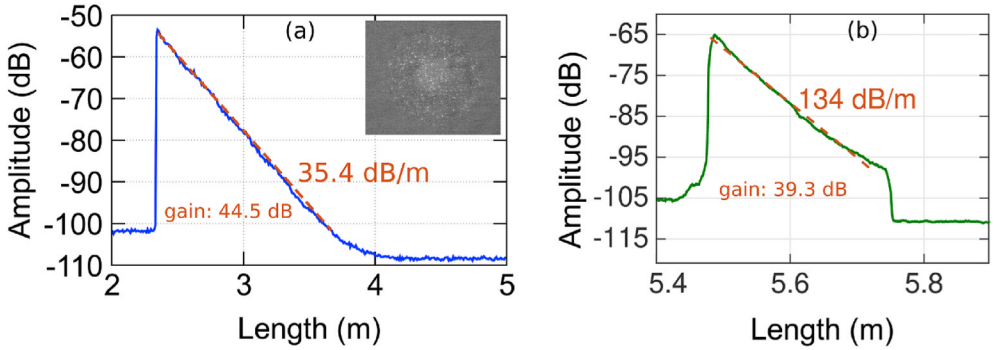

Fig. 1. Backscattering trace of NP-doped fiber: (a) fiber tagged as M01, in the inset the SEM of fiber cross-section; (b) Fiber tagged as R04.

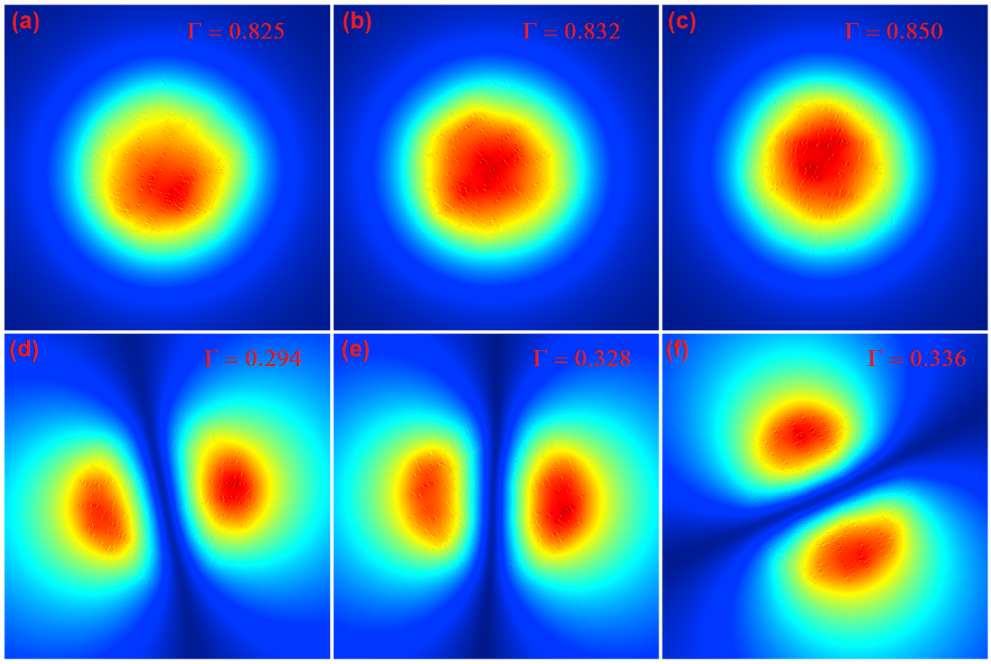

Fig. 2. Profile of the electric field of the Fundamental Mode (LP_{01}-like) for three different random nanoparticle distributions (a), (b) and (c); Profile of the most confined Higher Order Mode (LP_{11}-like) for three different random nanoparticle distributions (d), (e) and (f).

inscribe an FBG. The measured FBG reflection spectrum presents a shape that is typical of SM fibers with no artifact and no spectrum spreading that can induce to think to a multimode behavior.

2.3. Sensing applications

The high scattering is the key to implement the paradigm of SLMux, the solution to the intrinsic limitation of the OBR input, constrained to a single fiber sensor. The OBR, in order to detect the spectral shift given by the change of physical parameters like temperature and strain, implements a correlation between the spectral input and a spectrum of reference. If the backscattering comes from an input composed by a parallel of optical fibers, the OBR is not able to discriminate which fiber generates the shift. To overcome this limitation, the solution consists in the introduction in the optical parallel of cuts of NP-doped fiber, as sensing elements, overlapping only with SMF-28 pigtails. In this case, the OBR is able to distinguish the spectral shift, since the shift is given by the high-scattering NP-doped fiber. The other fibers in the parallel act as a background interference [15].

The capability of SLMux setup has been exploited for applications where a high density of sensing point is required in a compact space. These applications include, 2D thermal mapping during tumoral RF-ablation [16], and 3D shape sensing of medical needle [29]. Moreover, the high scattering properties of NP-doped fiber can be used to implement a mirrorless refractive index sensor, by etching the fiber, thus exposing the core [18,31]. Usually this kind of sensors are obtained by etching a reflective element inscribed, in the fiber core, like an FBG [7]. Here, the consistent backscattering is sufficient for reading both a variation of the backscattered intensity and a spectral shift induced by the presence of a surrounding analyte solution to sense.

3. Experimental setup

3.1. Loop with NP-doped fiber R04

The fiber loop has been implemented using a 50:50 1 × 2 splitter, while the sensing part has been built using a cut of R04 fiber. The schematic is shown in Fig. 3. The output of the Optical Backscattering Reflectometer (Luna OBR 4600) is connected to a single mode fiber pigtail 3 m long. After the pigtail, the loop is obtained by connecting the output of a 50:50 1 × 2 splitter to a sensing section, containing three cuts of fiber. The first and the third cuts are 2 SMF-28 connectorized pigtail of 34 cm and 43 cm respectively, while the central part is represented by a 32 cm long cut of R04 NP-doped fiber. All the connectors used in the

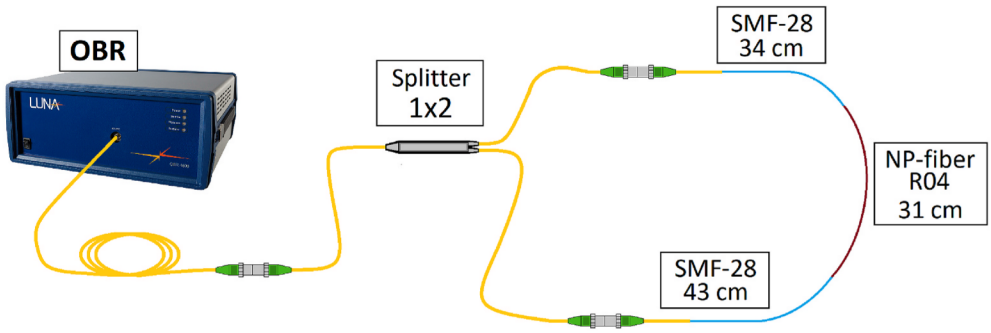

Fig. 3. Schematic of the fiber loop interferometer setup. The loop is connected to the OBR by a 3 m long pigtail. The loop is obtained by a 50:50 1 × 2 splitter, the output branches are connected to a sensing section containing a cut of R04 MgO NP-doped fiber.

setup are FC-APC type. The MgO NP-doped fiber has been spliced to the SMF-28 pigtails by using a standard telecom fiber (Fujikura 12S, SMF-SMF recipe).

It is worth noting that the presence of nanoparticles does not represent an impediment for the splicing operation, and a basic fusion splicer performs a more than decent job achieving splices with negligible losses. By taking in consideration the size and the concentration of the particles, the main material involved in the splicing procedure is silica, so that the optical properties of the splice are comparable to an SM-SM splice.

By considering the length of splitter pigtails, roughly 105 cm, and the length of the sensing part, the loop has a circumference 320 cm. The effect of the fiber loop is to create an interference pattern in the middle point of the loop. In fact, this configuration represents the fiber optic implementation of Sagnac interferometer.

The OBR laser output signal, characterized by a sweeping wavelength going form 1525 nm–1610 nm, is equally divided by the splitter. The two coherent, and equally distributed, signals are forced to interact each other in the middle point of the loop. The OBR can easily detect the backscattering peak generated by the interferent signals. The backscattering traces are shown in Fig. 4(a)-(b). The reference trace of the sensing element, measured when the loop is maintained open in one of its ends, is depicted in Fig. 4(a). Form the trace it is possible to see the typical sawtooth shape given by the presence of the NP-doped fiber. The scattering gain, with respect to the SMF-28 pigtail, is more than 39 dB, the two-way losses are measured to be 134 dB/m. From the plot we can see the lengths of the SMF-28 pigtails and the R04 cut, respectively of 34 cm, 43 cm, and 31 cm. By closing the loop, the OBR can detect the overlap of the backscattering traces, one given by the signal traveling the loop in clockwise direction and one given by the signal traveling in counterclockwise direction. It is possible to see, from Fig. 4(b), that in the middle point of the overlapped trace the interference pattern produces an additional peak of the backscattering. The peak is 37.4 dB larger than the NP-doped fiber backscattering and 78 dB larger that SMF-28 pigtail backscattering. It is worth noting that the backscattering trace presents two sawtooth, this is because the NP-doped fiber is not perfectly centered in the middle of the loop, so that one of the signal encounters one side of the NP-doped fiber before to merge with the other

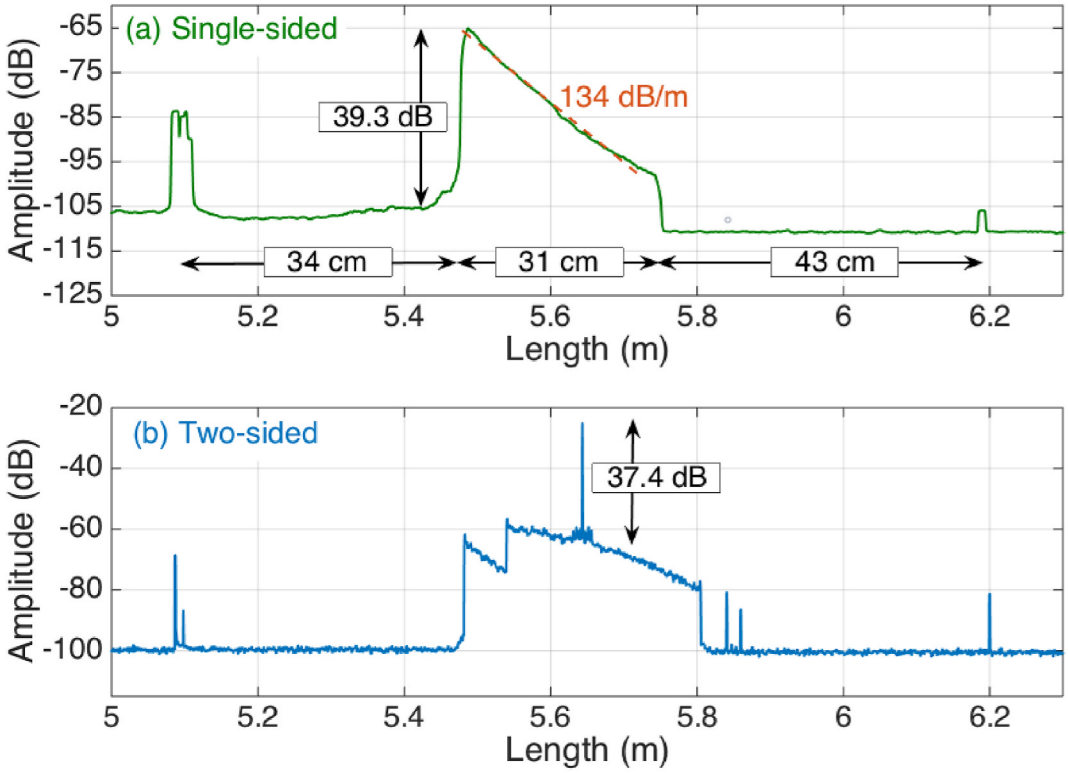

Fig. 4. Backscattering trace of fiber loop: (a) when the loop is open; (b) when the loop is closed.

signal propagating in the other direction. The large value of the backscattering is of great interest for all the sensing applications where a reflector structure is necessary [30], in this case the reflector-like behavior is achieved without a real reflector, but exploiting the properties of the high-scattering NP-doped fiber.

3.2. Thermal coefficient characterization setup

In order to characterize the temperature coefficient of the fiber loop, a simple setup has been built. The setup is shown in Fig. 5. The Luna OBR 4600 is connected to the fiber loop through a 3 m long pigtail, and the loop is created using a 50:50 1 × 2 splitter, as explained in the previous subsection. The sensing element is characterized by the presence of a cut of MgO NP-doped fiber.

The sensing element, in correspondence of the interferometer peak, has been placed on a thermal plate. The reference temperature has been taken by the help of an FBG, placed exactly on the same location of the NP-doped fiber interferometer peak. The FBG has been connected to the Micron Optics si255, a swept-laser interrogator, in order to precisely detect the temperature. A small glass baker has been positioned over the plate to enhance the uniformity of the air temperature around the sensors. Furthermore, the baker offers a protection form the air flow that the operator inevitably produces during the operation of measurement. With these precautions the temperature has been varied from the environment temperature of 23 °C to roughly 70 °C.

3.3. Strain coefficient characterization setup

The setup to characterize the strain is schematize in Fig. 6. In this setup the MgO NP-doped fiber sensor has been fixed between two movable stages in order to stretch the fiber. Two micro-positioners, with possibility of 1D manual linear movement, have been fixed to laboratory table, in front of each other, at a distance of 14 cm. The NP-doped fiber has been fixed to border of each micro-positioner by a small drop of cyanoacrylate based super-glue. The advantage of this kind of glue is mainly due to its stiffness, so that, after the application of the tension, the strain, possibly lost because of the elastic effect of the glue, is minimal. Moreover, this glue permits a solid fastening without damaging the fiber coating. An additional piece of strong tape has been put over the glued points to improve the stability of the system.

The strain has been applied by manually moving one the micro-positioner while holding the other one in its initial position. At each measurement, the distance between the positioners have been increased by a 10 μm. With this shift, fourteen steps correspond to strain of 1000 με. A total of twenty-one measurements have been taken, going form 0 με to roughly 1429 με.

4. Results and discussion

The Sagnac fiber loop configuration, combined with the special properties of high scattering MgO NP-doped fiber has been demonstrated to create a significant peak of backscattering, as shown in Fig. 4 (b). The peak appears in the position of the fiber loop where the split signals, one propagating in clockwise direction and the other propagating in the counterclockwise direction, interfere with each other. In Sagnac loop-based fiber sensors, one of the critical aspects is the capability to obtain a spectrum characterized by a clear interferometric pattern [2]. Because of several factors, including the presence of multi-mode propagation, the unpredictable polarization rotation, and the attenuation due to the bent losses, the onset of a well detectable spectrum can be difficult or impossible. The most used solution to overcome this issue is the use of a Polarization Maintaining (PM) fiber associated to a polarization control in the fiber loop, in order to cut the interfering modes to the number of two (the two polarization of the fundamental mode), with different propagation speed [19]. This solution appears valid, in particular when the loop is significantly longer than the wavelength.

OBR working principles are based on OFDR, which represents an advanced technology to achieve the analysis of reflection characteristics in optical fibers and components. OBR uses, as an input, a tunable laser source that sweeps over a band (in Luna OBR from 1525 nm to 1610 nm). The light that is reflected by the fiber under test is sent to interfere with a reference arm. By using the Fourier analysis of the interferent signal the time domain distribution of the reflected light is obtained. To pass to the spatial domain of the reflected light it is necessary to know the speed of light and the group velocity in the fiber. The source of reflection in the case of a SMF-28 is given by the intrinsic Rayleigh scattering of the glass, due to micro variation of the refractive index of the material. Since the Rayleigh scattering is deterministic, it represents a sort of signature of the fiber, showing point by point a well-defined backscattering spectrum [13].

This signature, constant in time, enable the distributed measurement of temperature and strain, since the variation of these parameters is detected as a shift of the spectrum, which can be detected by an operation of convolution with a reference signature. With the OBR technology, it is possible to achieve measurements with sub-millimeter resolution [5].

NP-doped fibers are characterized by a strong backscattering signature. Differently from SMF-28 the scattering is mainly given by the presence of nanoparticles. In terms of distributed sensing, the presence of Mg nanoparticles in the fiber core do not change the OBR principles. The spectral shift induced by changes of temperature and strain is similar to the one recorded using SMF-28. The reason is mainly because the mechanical and temperature properties of the fiber are dependent on

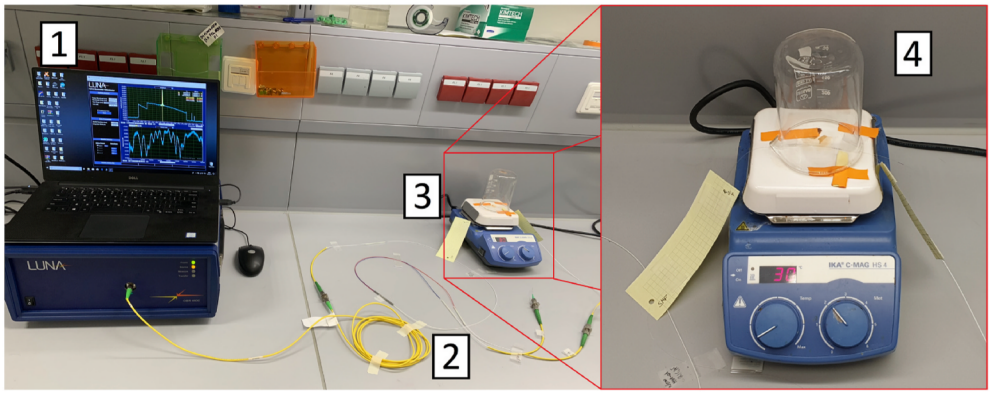

Fig. 5. Setup used for the thermal coefficient measurement of the fiber loop: (1) the Luna OBR 4600 and the laptop with the software; (2) 50:50 1 × 2 splitter; (3) thermal plate used for heating the fiber loop; (4) Detail of the thermal plate, the fiber loop is covered by a baker in order to homogenize the air temperature. The reference temperature is measured using an FBG interrogated by a swept-laser interrogator (Micron Optics si255).

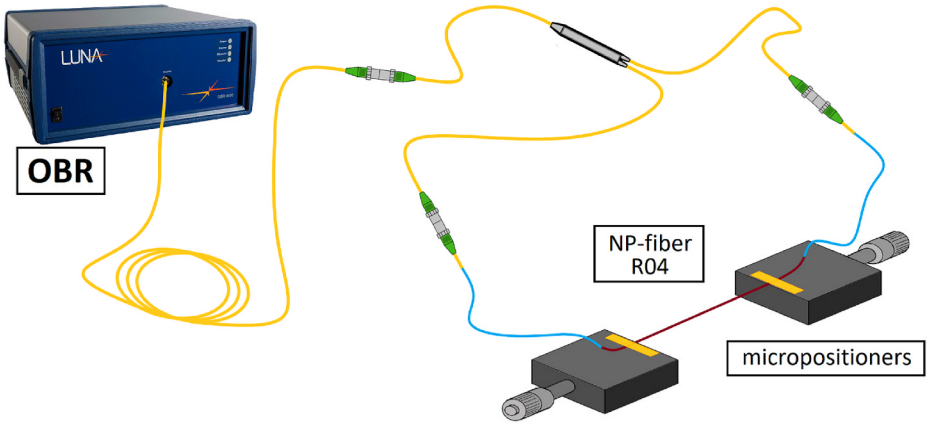

Fig. 6. Schematic of the setup used for the strain coefficient characterization. The NP-doped fiber is glued to two micro-positioners fixed to laboratory bench. The strain is imposed by acting on one of the micro-positioners.

the material, i.e. silica, which is dominant also in the Mg NP recipe. According to Blanc et al. [17], the size of the nanoparticles (between 15th to 30th times smaller than the wavelength) and index contrast with the surrounding medium induce a scattering of Rayleigh, with significant losses. The presence of a highly disordered pattern of nanoparticles, so close with each other, can foster the onset of localization phenomenon [32], and a local preservation of polarization [33]. These observations result beneficial for the formation of an interferometer pattern. In Fig. 7, the spectrum, calculated by the OBR is the proximity of the backscattering peak location, is depicted. The plot presents a recognizable pattern characterized by wavelength dependent hump and valley. Because of the strong disturbance introduced by the nanoparticles spectral pattern, the spectrum appears to be irregular. The amplitudes and the spatial distance of the fringes, expected in a Sagnac loop resonator, are not constant. Nevertheless, the spectral properties of loop are stable, since the NP scattering signature is deterministic, and the OBR results to be suitable for this kind of detection. The spectrum appears enough clear to be measured and used for sensing purpose.

The application of physical parameters changes, such as the application of strain to the NP-doped fiber cut, induces a shift in the spectrum, as shown in Fig. 7. The spectrum shift can be detected by different methods, one is represented by the correlation of the entire spectrum with a reference spectrum in order to detect the average shift on the band between 1525 nm and 1610 nm, the second in the peak tracking of the most significant peak in the spectrum. As shown in Fig. 7 inset, the spectrum presents a clear minimum located at 1537 nm. This point of minimum is sensitive to the application of strain and it clearly shifts toward the longer wavelength with the increase of applied strain.

The analysis of the experimental results, depicted in Fig. 8, shows the dependency of the wavelength shift as a function of the applied strain. The dependency is linear, and the fit curve presents a coefficient of determination R^2 equal to 0.99. The strain coefficient, namely the wavelength shift over the applied strain, of the Sagnac fiber loop is measured to be 1.93 p.m./με. Similar conclusion can be reached by testing the fiber loop for temperature detection. As shown in Fig. 9, the experimental results of the wavelength shift versus the temperature fit a good linear approximation (R^2 equal to 0.98), and the thermal coefficient can be determined to a value of 1.75 p.m./°C.

The coefficients of strain and temperature calculated in the analysis of NP-doped loop configuration show interesting properties compared to a standard SMF-28 when used as a distributed sensor. We can notice that the strain coefficient is higher with a value of 1.93 p.m./με versus 1.2 p.m./με, while the temperature coefficient is significantly lower (1.75 p.m./°C versus 10.5 p.m./°C) [14], this is due by the fact that the loop configuration with enhanced backscattering given by the presence of Mg nanoparticles, is less sensitive to the temperature with respect to the strain. This opens an interesting perspective in sensing capability combining the fiber loop with other fiber optic devices that can be easily detected by the OBR system. This difference between strain and temperature coefficient can be also used, in combination with the same fiber

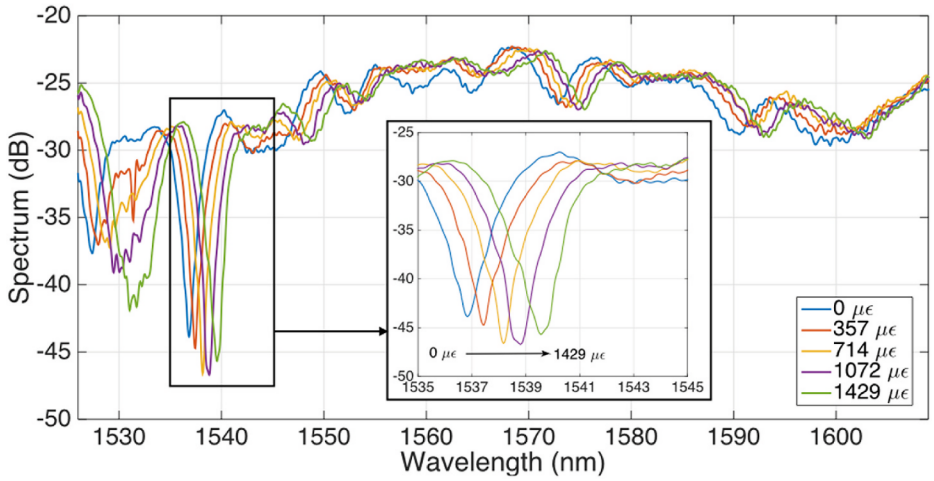

Fig. 7. Whole spectrum of the interferometer peak obtained by the Signac configuration of the loop. The spectrum presents a red shift by applying a strain. (For interpretation of the references to colour in this figure legend, the reader is referred to the Web version of this article.)

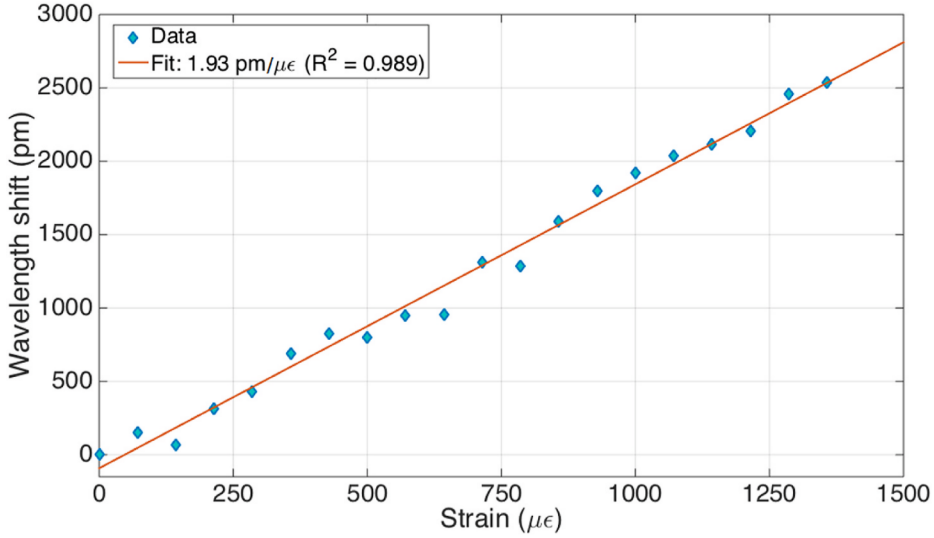

Fig. 8. Measured wavelength shift vs strain. The linear fit, presenting a high coefficient of determination, is shown using a red line. (For interpretation of the references to colour in this figure legend, the reader is referred to the Web version of this article.)

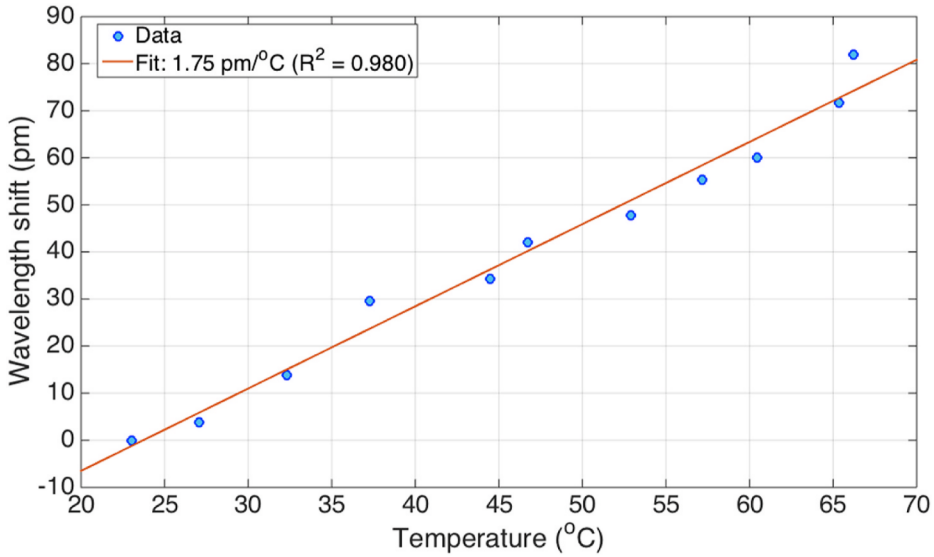

Fig. 9. Measured wavelength shift vs temperature. The linear fit, presenting a high coefficient of determination, is shown using a red line. (For interpretation of the references to colour in this figure legend, the reader is referred to the Web version of this article.)

NP-fiber, to discriminate the simultaneous measurement of temperature and strain [34]. Another interesting aspect of this particular technology, merging the properties of the Sagnac loop configuration, strengthen by the presence of high scattering NP-doped fiber, and the detection capability of the OBR systems, is the possibility of creating a network of sensors presenting a good grade of flexibility in terms of, compactness, network configuration, and scalability of the sensing system [35].

5. Conclusions

A Sagnac fiber loop sensor, where the sensing element consists of a special, custom made, MgO NP-doped fiber, has been implemented and investigated by using an OBR system (Luna OBR 4600). The custom fiber has been drawn from a preform obtained by a conventional MCVD, and the formation of nanoparticles comes from a technological process based on spontaneous phase separation between alkaline earth and silica substrate. The presence of a random pattern of nanoparticles in the fiber core highly increases the fiber backscattering, which is nearly 40 dB higher than the backscattering of standard SMF-28 telecom optical fiber. The fiber attenuation increases too, showing an average value of 134 dB/m. The high backscattering promotes the formation of a strong fiber spectral signature, well-detectable by the OBR system. Moreover, the high-scattering properties of the fiber, locally combined with a well-defined polarization state, are beneficial for the Sagnac fiber loop configuration.

In this work a fiber loop of 320 cm has been created using a 50:50 1 $\times$ 2 splitter. The central part of the loop is occupied by a cut of NP-doped fiber. The middle point of the loop, where the clockwise and the counterclockwise input signal encounter each other, presents an additional increase of the backscattering, 37.4 dB higher than the NP-doped fiber and roughly 78 dB higher than a standard SMF-28 fiber. The spectral analysis of the high backscattering location, performed by the OBR, has shown a clear, although noisy, interferometer pattern. Further investigations have demonstrated the consistent possibility of using this fiber loop system as a sensor, since the interferometer spectrum can shift by changing temperature and strain applied to the NP-doped fiber. The

spectral shift, detectable with spectral correlation or with peak tracking, is linear with the variation of both temperature and strain. The measured temperature and strain coefficients are respectively 1.75 p.m./°C and 1.93 p.m./με. These coefficients are significantly different from the correspondent one shown by standard telecom SMF-28 silica-based fiber. This is of interest for sensors system that intends to combine different optical fiber devices. Moreover, this peculiar property can be exploited to discriminate the simultaneous measurement of temperature and strain.

Declaration of competing interest

The authors declare that they have no known competing financial interests or personal relationships that could have appeared to influence the work reported in this paper.

CRediT authorship contribution statement

Carlo Molardi: Methodology, Investigation, Visualization, Funding acquisition, Writing - original draft. **Wilfried Blanc:** Resources, Writing - review & editing. **Daniele Tosi:** Conceptualization, Methodology, Investigation, Visualization.

Acknowledgments

The research was funded by Nazarbayev University, under grants SMARTER (code: 091019CRP2117), EPICGuide (code: 240919FD3908), and FOSTHER (code: 090118FD5314). This work was partly supported by ANR Project NanoSlim (ANR-17-CE08-0002). The authors thank Michèle Ude and Stansilaw Trzesien (INPHYNI, Nice, France), for the preparation of the preforms and the fibers.

References

[1] B. Lee, Review of the present status of optical fiber sensors, Opt. Fiber Technol. 9 (2) (2003) 57–79.
[2] E. Udd, W.B. Spillman Jr., Fiber Optic Sensors: an Introduction for Engineers and Scientists, John Wiley & Sons, 2011.
[3] H. Joe, H. Yun, S. Jo, M.B.G. Jun, B. Min, A review on optical fiber sensors for environmental monitoring, Int. J. of Precis. Eng. and Manuf.-Green Tech. 5 (2018) 173–191.
[4] Biological Evaluation of Medical Devices, ISO 10993, International Organization for Standardization, Geneva, Switzerland, 1995.
[5] D. Tosi, E. Schena, C. Molardi, S. Korganbayev, Fiber optic sensors for sub-centimeter spatially resolved measurements: review and biomedical applications, Opt. Fiber Technol. 43 (2018) 6–19.
[6] Y.J. Rao, Recent progress in applications of in-fibre Bragg grating sensors, Optic Laser. Eng. 31 (4) (1999) 297–324.
[7] A. Iadicicco, A. Cusano, S. Campopiano, A. Cutolo, M. Giordano, Thinned fiber Bragg gratings as refractive index sensors, IEEE Sensor. J. 5 (6) (2005) 1288–1295.
[8] A. Bekmurzayeva, K. Dukenbayev, M. Shaimerdenova, I. Bekniyazov, T. Ayupova, M. Sypabekova, C. Molardi, D. Tosi, Etched fiber Bragg grating biosensor functionalized with aptamers for detection of thrombin, Sensors 18 (12) (2018) 4298.
[9] B. Lee, S. Roh, J. Park, Current status of micro- and nano-structured optical fiber sensors, Opt. Fiber Technol. 15 (3) (2009) 209–221.
[10] O.S. Wolfbeis, Fiber-optic chemical sensors and biosensors, Anal. Chem. 80 (12) (2008) 4269–4283.
[11] W. Jin, "Multiplexed FBG Sensors and Their Applications," Proc. SPIE 3897, Advanced Photonic Sensors and Applications, 1999.
[12] X. Bao, L. Chen, Recent progress in distributed fiber optic sensor, Sensors 12 (7) (2012) 8601–8639.
[13] M. Froggatt, J. Moore, High-spatial-resolution distributed strain measurement in optical fiber with Rayleigh scatter, Appl. Optic. 37 (10) (1998) 1735–1740.
[14] Luna technologies, OBR 4600 [Online]. Available: http://lunainc.com/product/sensing-solutions/obr-4600.
[15] A. Beisenova, A. Issatayeva, S. Korganbayev, C. Molardi, W. Blanc, D. Tosi, Simultaneous distributed sensing on multiple MgO-doped high scattering fibers by means of scattering-level multiplexing, J. Lightwave Technol. 37 (13) (2019) 3413–3421.
[16] A. Beisenova, A. Issatayeva, S. Sovetov, S. Korganbayev, M. Jelbuldina, Z. Ashikbayeva, W. Blanc, E. Schena, S. Sales, C. Molardi, D. Tosi, Multi-fiber distributed thermal profiling of minimally invasive thermal ablation with scattering-level multiplexing in MgO-doped fibers, Biomed. Optic Express 10 (3) (2019) 1282–1296.
[17] W. Blanc, V. Mauroy, L. Nguyen, B.N. Shivakiran Bhaktha, P. Sebbah, B.P. Pal, B. Dussardier, "Fabrication of rare earth-doped transparent glass ceramic optical fibers by modified chemical vapor deposition, J. Am. Ceram. Soc. 94 (8) (2011) 2315–2318.
[18] S. Korganbayev, M. Shaimerdenova, T. Ayupova, M. Sypabekova, A. Bekmurzayeva, W. Blanc, C. Molardi, D. Tosi, Refractive index sensor by interrogation of etched MgO nanoparticle-doped optical fiber signature, Photon. Technology Lett. 31 (15) (2019) 1253–1256.
[19] B.H. Lee, Y.H. Kim, K.S. Park, J.B. Eom, M.J. Kim, B.S. Rho, H.Y. Choi, Interferometric fiber optic sensors, Sensors 12 (3) (2012) 2467–2486.
[20] H.Y. Fu, H.Y. Tam, L.Y. Shao, X. Dong, P.K.A. Wai, C. Lu, S.K. Khijwania, Pressure sensor realized with polarization-maintaining photonic crystal fiber-based Sagnac interferometer, Appl. Optic. 47 (2008) 2835–2839.
[21] H.J. Arditty, H.C. Lefevre, Sagnac effect in fiber optic gyroscopes, Opt. Lett. 6 (1981) 401–403.
[22] D.S. Moon, B.H. Kim, A. Lin, G. Sun, T.G. Han, W.T. Han, Y. Chung, The temperature sensitivity of Sagnac loop interferometer based on polarization maintaining side-hole fiber, Optic Express 15 (2007) 7962–7967.
[23] X.Y. Dong, H.Y. Tam, P. Shum, Temperature-insensitive strain sensor with polarization-maintaining photonic crystal fiber based Sagnac interferometer, Appl. Phys. Lett. 90 (15) (2007) 151113.
[24] E. Udd, "Fiber-Optic Acoustic Sensor Based on the Sagnac Interferometer," Proc. SPIE 0425, Single Mode Optical Fibers, 1983.
[25] T.K. Gangopadhyay, J.V. Ittiarah, Recent advances in fiber loop ringdown sensors, Optic. Sci. Eng.: Springer Proc. Phys. 194 (2007) 117–125.
[26] W. Blanc, B. Dussardier, Formation and applications of nanoparticles in silica optical fibers, J. Optic. 45 (3) (2016) 247–254.
[27] M. Vermillac, H. Fneich, J. Turlier, M. Cabié, C. Kucera, D. Borschneck, F. Peters, P. Vennéguès, T. Neisius, S. Chaussedent, D.R. Neuville, A. Mehdi, J. Ballato, W. Blanc, On the morphologies of oxides particles in optical fibers: effect of the drawing tension and composition, Opt. Mater. 87 (2019) 74–79.
[28] W. Blanc, I. Martin, H. François-Saint-Cyr, X. Bidault, S. Chaussedent, C. Hombourger, S. Lacomme, P. Le Coustumer, D.R. Neuville, D.J. Larson, T. J. Prosa, C. Guillermier, Compositional changes at the early stages of nanoparticles growth in glasses, J. Phys. Chem. C 123 (2019) 29008–29014.
[29] C. Molardi, T. Paixão, A. Beisenova, R. Min, P. Antunes, C. Marques, W. Blanc, D. Tosi, Fiber Bragg grating (FBG) sensors in a high-scattering optical fiber doped with MgO nanoparticles for polarization-dependent temperature sensing, Appl. Sci. 9 (2019) 3107.
[30] A. Beisenova, A. Issatayeva, I. Iordachita, W. Blanc, C. Molardi, D. Tosi, Distributed fiber optics 3D shape sensing by means of high scattering NP-doped fibers simultaneous spatial multiplexing, Optic Express 27 (16) (2019) 22074–22087.
[31] T. Ayupova, M. Shaimerdenova, S. Korganbayev, M. Sypabekova, A. Bekmurzayeva, W. Blanc, S. Sales, T. Guo, C. Molardi, Daniele Tosi, Fiber optic reflector-less refractive index distributed multi-sensors by scattering-level multiplexing with MgO nanoparticle-doped fibers, IEEE Sensor. J. 20 (5) (2020) 2504–2510.
[32] B. Abaie, E. Mobini, S. Karbasi, T. Hawkins, J. Ballato, A. Mafi, Random lasing in an Anderson localizing optical fiber, Light Sci. Appl. 6 (2017) 17041.
[33] C. Molardi, S. Korganbayev, W. Blanc, D. Tosi, Characterization of a nanoparticles-doped optical fiber by the use of optical backscatter reflectometry, Proc. SPIE, SPIE/COS Photonics Asia 10821 (2018) 1082121.
[34] O. Frazao, J.L. Santos, J.M. Baptista, Strain and temperature discrimination using concatenated high-birefringence fiber loop mirrors, IEEE Photon. Technol. Lett. 19 (2007) 1260–1262.
[35] M.T.M.R. Giraldi, C.S. Fernandes, M.S. Ferreira, M.J. De Sousa, P.A.S. Jorge, J. Crisostomo, W.A. Costa, J.L.C.O. Santos, O. Frazao, Fiber loop mirror sensors interrogated and multiplexed by OTDR, J. Lightwave Technol. 33 (12) (2015) 2580–2584.